

Article

Crystal Structure and Functional Characterization of an S-Formylglutathione Hydrolase (*BuSFGH*) from *Burkholderiaceae* sp.

Jisub Hwang^{1,2,†} , Hackwon Do^{1,2,†}, Youn-Soo Shim^{3,*}  and Jun Hyuck Lee^{1,2,*} 

¹ Research Unit of Cryogenic Novel Material, Korea Polar Research Institute, Incheon 21990, Republic of Korea; hjsub9696@kopri.re.kr (J.H.); hackwondo@kopri.re.kr (H.D.)

² Department of Polar Sciences, University of Science and Technology, Incheon 21990, Republic of Korea

³ Department of Dental Hygiene, Sunmoon University, Asan 31460, Republic of Korea

* Correspondence: shim-21@hanmail.net (Y.-S.S.); junhyucklee@kopri.re.kr (J.H.L.);

Tel.: +82-41-530-2740 (Y.-S.S.); +82-32-760-5555 (J.H.L.); Fax: +82-41-530-2726 (Y.-S.S.); +82-32-760-5509 (J.H.L.)

† These authors contributed equally to this work.

Abstract: S-formylglutathione hydrolases (SFGHs) catalyze the hydrolysis of S-formylglutathione to formate and glutathione using the conserved serine hydrolase catalytic triad residues (Ser-His-Asp). SFGHs have broad substrate specificity, including, for example, ester bond-containing substrates. Here, we report the crystal structure of *Burkholderiaceae* sp. SFGH (*BuSFGH*) at 1.73 Å resolution. Structural analysis showed that the overall structure of *BuSFGH* has a typical α/β hydrolase fold, with a central β -sheet surrounded by α -helices. Analytical ultracentrifugation analysis showed that *BuSFGH* formed a stable dimer in solution. The enzyme activity assay indicated that *BuSFGH* has a high preference for short-chain *p*-nitrophenyl esters, such as *p*-nitrophenyl acetate. The activity of *BuSFGH* toward *p*-nitrophenyl acetate was five times higher than that of *p*-nitrophenyl butylate. Molecular modeling studies on the *p*-nitrophenyl acetate-bound *BuSFGH* structure indicate that Gly52, Leu53, Trp96, His147, Ser148, Trp182, Phe228, and His259 residues may be crucial for substrate binding. Collectively, these results are useful for understanding the substrate-binding mechanism and substrate specificity of *BuSFGH*. They can also provide useful insights for designing modified *BuSFGH*s with different substrate specificities.

Keywords: crystal structure; dimer; S-formylglutathione hydrolase; X-ray crystallography



Citation: Hwang, J.; Do, H.; Shim, Y.-S.; Lee, J.H. Crystal Structure and Functional Characterization of an S-Formylglutathione Hydrolase (*BuSFGH*) from *Burkholderiaceae* sp.. *Crystals* **2023**, *13*, 621. <https://doi.org/10.3390/cryst13040621>

Academic Editors: Bo Liang and Houfu Guo

Received: 11 March 2023

Revised: 28 March 2023

Accepted: 2 April 2023

Published: 4 April 2023



Copyright: © 2023 by the authors. Licensee MDPI, Basel, Switzerland. This article is an open access article distributed under the terms and conditions of the Creative Commons Attribution (CC BY) license (<https://creativecommons.org/licenses/by/4.0/>).

1. Introduction

S-formylglutathione hydrolases (SFGHs; also, esterase D) catalyze the hydrolysis of S-formylglutathione substrate to two products (formate and glutathione) with a canonical serine hydrolase catalytic triad (Ser-Asp-His). SFGHs are present in many prokaryotes and eukaryotes, and their biological function may be related to the formaldehyde detoxification process [1–4]. A SFGHs sequence analysis from various sources revealed that SFGHs have a conserved sequence motif (GHSMGG) near the active site [5,6]. This sequence motif harbors a catalytic Ser residue. Notably, SFGHs have another strictly conserved Cys residue near the substrate-binding site. This Cys residue may play an important role in determining the substrate specificity and functional regulation of SFGHs [1,3]. Under oxidative conditions, S-glutathionylation of regulatory cysteine induces protein inactivation [7,8]. Thus, the conserved Cys residue is speculated to interact with the thioester product and form a covalent linkage for feedback inhibition. However, the exact biological function and regulatory mechanism of Cys residues in SFGHs remain unclear. Moreover, recent studies have revealed that SFGHs have a broad substrate specificity spectrum [9–12]. They can hydrolyze various ester bond-containing substrates, including *p*-nitrophenyl esters and xenobiotic carboxyesters.

We conducted structural and biochemical studies on several bacterial SFGHs, and previously determined the crystal structure of a novel cold-active S-formylglutathione hydrolase (*SfSFGH*) homolog from the psychrophilic bacterium (*Shewanella frigidimarina*) [9]. Structure-based mutagenesis studies revealed that the W182A mutant alters the substrate specificity of *SfSFGH*. Another study established the structure and biochemical characterization of an S-formylglutathione hydrolase (*VaSFGH*) from *Variovorax* sp. PAMC 28,711 (a bacterium isolated from an Antarctic lichen) [12]. Furthermore, comparative modeling studies using various *p*-nitrophenyl ester substrates revealed that large, long substrates could not bind inside the small, static, hydrophobic substrate-binding pocket owing to the static and small size of the substrate-binding pocket of *VaSFGH*. *SfSFGH* and *VaSFGH* structural analyses revealed that these proteins share a high degree of structural similarity and oligomerization as dimers in solution. Activity assays revealed that both *SfSFGH* and *VaSFGH* exhibited high activity towards short-chain *p*-nitrophenyl esters (C2–C6), and that this activity decreased as the length of the substrate increased.

In this study, we determined the X-ray crystal structure of the *Burkholderiaceae* sp. S-formylglutathione hydrolase (*BuSFGH*) homolog, then performed structural analysis and enzyme activity assays. The results revealed that *BuSFGH* prefers substrates with short acyl chains, similar to other SFGHs. Molecular modeling studies were performed to better understand the substrate specificity of *BuSFGH*, its interactions with *p*-nitrophenol acetate, and its preference for *p*-nitrophenol acetate over *p*-nitrophenyl butylate. These findings provide useful information for understanding the substrate recognition mechanism of *BuSFGH* and provide insights for the protein engineering of this enzyme.

2. Materials and Methods

2.1. *BuSFGH* Cloning, Expression, and Purification

The S-formylglutathione hydrolase gene, discovered in *Burkholderiaceae*, was synthesized and cloned into a pET28a vector (Bioneer, Daejeon, Korea) using *Nde*I and *Xho*I restriction enzyme sites. The recombinant plasmid was then transformed into *Escherichia coli* BL21 (DE3) cells for protein expression. The recombinant cells were grown in 2 L of lysogeny broth (LB) medium containing 50 $\mu\text{g mL}^{-1}$ kanamycin at 37 °C. At an optical density (OD) of 0.6 (OD₆₀₀), 0.5 mM isopropyl-1-thio- β -D-galactopyranoside (IPTG) was added, and the cells were cultured overnight at 25 °C. The cells were harvested by centrifugation at 6000 rpm for 20 min and resuspended in cell lysis buffer (50 mM sodium phosphate, 300 mM NaCl, and 5 mM imidazole, pH 8.0). After sonication on ice, the supernatant was collected and loaded onto a pre-equilibrated Ni-NTA column. Next, the protein-bound resin was washed with wash buffer (50 mM sodium phosphate, 300 mM NaCl, and 30 mM imidazole, pH 8.0). Finally, the bound proteins were eluted using an elution buffer (50 mM sodium phosphate, 300 mM NaCl, and 300 mM imidazole, pH 8.0). The eluted protein fraction was incubated with thrombin protease to cleave the 6X-histidine tag. Finally, size-exclusion chromatography was performed to purify single-targeted *BuSFGH*, and the enzyme was concentrated to 51.8 mg/mL.

2.2. Substrate Specificity and Optimal Conditions for Enzymatic Activity

Substrate specificity was investigated using varying lengths of *p*-nitrophenyl esters, including *p*-nitrophenyl acetate (*p*-NA, C2), *p*-nitrophenyl butylate (*p*-NB, C4), *p*-nitrophenyl valerate (*p*-NV, C5), *p*-nitrophenyl octanoate (*p*-NO, C8), and *p*-nitrophenyl decanoate (*p*-ND, C10). For the enzymatic reaction, 10 μg of purified *BuSFGH* and 250 μM of a single substrate were mixed in a 20 mM Tris-HCl (pH 8.0) and 200 mM NaCl solution. The enzymatic activity was measured at 25 °C, and the amount of generated *p*-nitrophenol (the reaction product) was monitored at 405 nm. The enzymatic reaction with *p*-nitrophenyl acetate was defined as 100%. The optimal temperature was determined using varied temperatures from 4 °C to 60 °C. The optimal pH was determined using reaction buffers with different pH values: Sodium citrate (pH 3–5), sodium phosphate (pH 6–7), Tris-HCl (pH 7.5 to 8.5), CHES (pH 9.0 to 9.5), and CAPS (pH 10–11). *P*-NA (C2) was used as the substrate to

investigate the optimal temperature and pH conditions. All experiments were performed in triplicate using a 10 mm quartz cuvette cell. All figures were generated using the Prism software (version 5).

2.3. Crystallization, X-ray Diffraction, and Structure Determination

The initial screening for *BuSFGH* crystallization was performed using a Mosquito crystallization robot (TTP LabTech, Melbourn, UK) via sitting-drop vapor diffusion at 23 °C. Commercially available crystallization-screening solution kits were used, including the MCSG 1T to 4T (Anatrace, Maumee, USA), SaltRx, and Index (Hampton Research, Aliso Viejo, CA, USA) kits. The protein solution was mixed with the crystallization solution at a 1:1 ratio and equilibrated against 70 µL of the reservoir solution. The *BuSFGH* crystals appeared after 2 days at the following conditions: 0.2 M ammonium citrate, pH 5.0, and 20% (*w/v*) PEG 3350 with 31 mg/mL of protein. A single crystal was briefly soaked in Paratone-N oil for cryoprotection before crystal mounting on the synchrotron. X-ray diffraction data were collected on a BL-5C beam line of the Pohang Accelerator Laboratory (PAL, Pohang, Korea) with an oscillation of 1° per image. Data containing 360 images were indexed, integrated, and scaled using HKL-2000 software [13]. The number of molecules in the asymmetric unit was estimated using the Matthews coefficient value [14]. The crystal structure of *BuSFGH* was solved using the molecular replacement method using *MOLREP* from *CCP4i* suite [15,16]. The crystal structure of human esterase D (PDB code 3FCX) was used as a template model. Subsequently, the initial solution model was iteratively rebuilt and refined using *Coot* [17], *REFMAC* [18], and *phenix.refine* [19]. The final model was validated using *Molprobity* [20]. The structural refinement statistics are presented in Table 1. Structural figures were generated using *PyMOL* [21]. The detailed X-ray diffraction data collection and structural refinement statistics are presented in Table 1. The coordinate and structural factors of *BuSFGH* were deposited in the Protein Data Bank under the accession code 8ILJ.

Table 1. X-ray diffraction data collection and refinement statistics.

Data Set	<i>BuSFGH</i>
X-ray source	PAL-5C
Space group	$P2_12_12_1$
Unit-cell parameters (Å, °)	A = 50.37, b = 109.29, c = 112.62, $\alpha = \beta = \gamma = 90$
Wavelength (Å)	0.9796
Resolution (Å)	29.52–1.73 (1.76–1.73)
Total reflections	816,722 (85260)
Unique reflections	65,529 (6421)
Average I/ σ (I)	20.63 (6.17)
R_{merge} ^a	0.081 (0.397)
Redundancy	12.5 (13.3)
CC(1/2)	0.999 (0.969)
Completeness (%)	99.7 (98.9)
Refinement	
Resolution range (Å)	29.52–1.73 (1.79–1.73)
No. of reflections of working set	65,525 (6428)
No. of reflections of test set	3277 (322)
No. of amino acid residues	562
No. of water molecules	416
R_{cryst} ^b	0.195 (0.225)
R_{free} ^c	0.210 (0.237)
R.m.s. bond length (Å)	0.011

Table 1. Cont.

Data Set	BuSFGH
R.m.s. bond angle (°)	1.15
Average B value (Å ²) (protein)	20.12
Average B value (Å ²) (solvent)	27.49

^a $R_{\text{merge}} = \sum | \langle I \rangle - I | / \sum \langle I \rangle$. ^b $R_{\text{cryst}} = \sum | |F_o| - |F_c| | / \sum |F_o|$. ^c R_{free} calculated with 5% of all reflections excluded from refinement stages using high-resolution data. Values in parentheses refer to the highest-resolution shells.

2.4. Analytical Ultracentrifugation (AUC) and Interface Analysis

The oligomerization state of BuSFGH was investigated via AUC using Proteome Lab XL-A (Beckman Coulter). BuSFGH was prepared in 50 mM sodium phosphate, 300 mM NaCl (pH 8.0), and 200 mM NaCl buffers. The samples were centrifuged at 40,000 rpm for 10 min at 20 °C. The sedimentation profile of BuSFGH was monitored at 280 nm and the data were analyzed using the SEDFIT software [22]. PISA was used to analyze the interfacial residues and area of BuSFGH [23].

2.5. Molecular Docking Simulation

Molecular docking simulations were performed to predict protein–ligand interactions and investigate substrate-binding residues. AutoDock 4.2.1 [24] and jLigand [25] software were used for docking simulation and ligand generation, respectively. *p*-nitrophenyl acetate was used as the ligand for docking with BuSFGH. BuSFGH was prepared as a monomer without water molecules, and polar hydrogen atoms were further added using AutoDock Tools [24]. Molecular docking simulation was performed using AutoDock Vina [26] with the Lamarckian genetic algorithm, and the generated complex structure was visualized using PyMOL software [21].

3. Results and Discussion

3.1. Recombinant Protein Expression, Crystallization, and X-ray Diffraction of BuSFGH

S-Formylglutathione hydrolase from *Burkholderiaceae* sp. (BuSFGH; NCBI Accession Number: WP_062000720) consisted of 281 amino acid residues (calculated molecular weight of 30,802 Da) and had a theoretical isoelectric point of 6.05. The BuSFGH gene was successfully cloned, overexpressed, and purified (Figure 1A,B). The enzyme purification typically yielded approximately 100 mg/L, and the protein was concentrated to 51.8 mg/mL. The BuSFGH crystals formed within 2 days under an optimized buffer condition: 0.2 M ammonium citrate, pH 5.0, and 20% (*w/v*) PEG 3350. The BuSFGH crystal (Figure 1C) belonged to space group P2₁2₁2₁ and had unit-cell parameters $a = 50.37 \text{ \AA}$, $b = 109.29 \text{ \AA}$, $c = 112.62 \text{ \AA}$, and $\alpha = \beta = \gamma = 90^\circ$. A representative X-ray diffraction image of a BuSFGH crystal is shown in Figure 1D. Assuming the presence of a dimer in the asymmetric unit, the Matthews coefficient value was calculated to be $2.52 \text{ \AA}^3 \text{ Da}^{-1}$, which corresponds to a solvent content of 51.14%.

3.2. BuSFGH Activity Assay and Substrate Specificity

An enzyme activity assay of BuSFGH was performed using *p*-nitrophenyl esters of various fatty acid chain lengths, such as *p*-nitrophenyl acetate (*p*-NA, C2), *p*-nitrophenyl butylate (*p*-NB, C4), *p*-nitrophenyl valerate (*p*-NV, C5), *p*-nitrophenyl octanoate (*p*-NO, C8), and *p*-nitrophenyl decanoate (*p*-ND, C10). The enzyme showed the highest activity toward *p*-NA, whereas hydrolytic activity decreased dramatically as the length of the substrate increased. The hydrolytic activity of *p*-NB was 90% lower than that of *p*-NA (set at 100%) (Figure 2A). Thus, BuSFGH prefers short-chain ester compounds as substrates. It should be noted that SfSFGH and VaSFGH prefer short-length substrates, but their enzyme activity gradually decreases as the length of the substrate increases. Next, the optimal pH and temperature of BuSFGH were monitored in the pH range of 3.0 to 10.0, and temperature range of 4 °C to 60 °C, using *p*-NA as a substrate. The optimal pH was 8.0 for BuSFGH

activity, and enzyme activity rapidly decreased at pH 9.0, reaching approximately 50% of its maximum activity (Figure 2B). The optimal temperature for *BuSFGH* activity was 45 °C (Figure 2C), and there was a sharp reduction in activity as the temperature increased to above 50 °C.

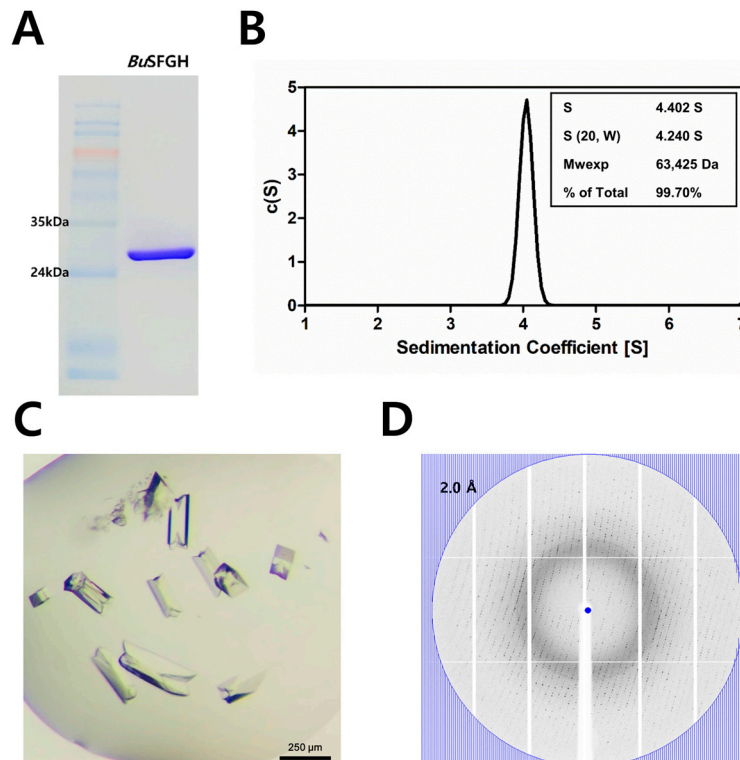


Figure 1. Recombinant *Burkholderiaceae* sp. S-formylglutathione hydrolase (*BuSFGH*) protein purification, crystallization, and X-ray diffraction data collection. (A) Sodium dodecyl-sulfate polyacrylamide gel electrophoresis (SDS-PAGE) analysis using finally purified *BuSFGH* protein. (B) The analytical ultracentrifugation (AUC) result shows purified *BuSFGH* protein exists as dimer in solution. (C) *BuSFGH* crystals were obtained under optimized conditions of 0.2 M ammonium citrate, dibasic pH 5.0, and 20% (*w/v*) PEG 3350, and were used for X-ray diffraction data collection. (D) Representative X-ray diffraction image using a *BuSFGH* crystal is shown with the 2.0 Å resolution value circle.

3.3. Overall Structure of *BuSFGH*

The crystal structure of *BuSFGH* was determined to belong to the $P2_12_12_1$ space group. As a template model, we used the crystal structure of Homo sapiens esterase D (PDB code 3FCX) with a molecular replacement method. The final model was refined to 1.73 Å and produced R_{work} and R_{free} values of 0.195 and 0.210, respectively (Table 1). The overall structure of the *BuSFGH* monomer is composed of 9 β-strands surrounded by 12 α-helices, which corresponds to a typical αβ-hydrolase fold (Figure 3). The asymmetric unit of the *BuSFGH* crystal contains two protomers with 416 water molecules. The results of analytical ultracentrifugation demonstrated that the purified *BuSFGH* protein formed a stable dimer in solution (Figure 1B). The dimer interface in *BuSFGH* was formed mainly by hydrogen bonds (His8-Asp258, Phe11-Tyr257, Arg9-Glu255, Arg9-Tyr257, Phe11-Tyr257, Phe11-Thr266, Ser12-Tyr257, Glu58-Tyr262, Gly65-Arg68, and Tyr257-Asp258). The dimer interface occupies 944.4 Å² of the total surface area of 11523.7 Å² of each monomer subunit (Figure 4). The structurally homologous proteins were investigated using the Dali-Lite server [27] and are summarized in Table 2.

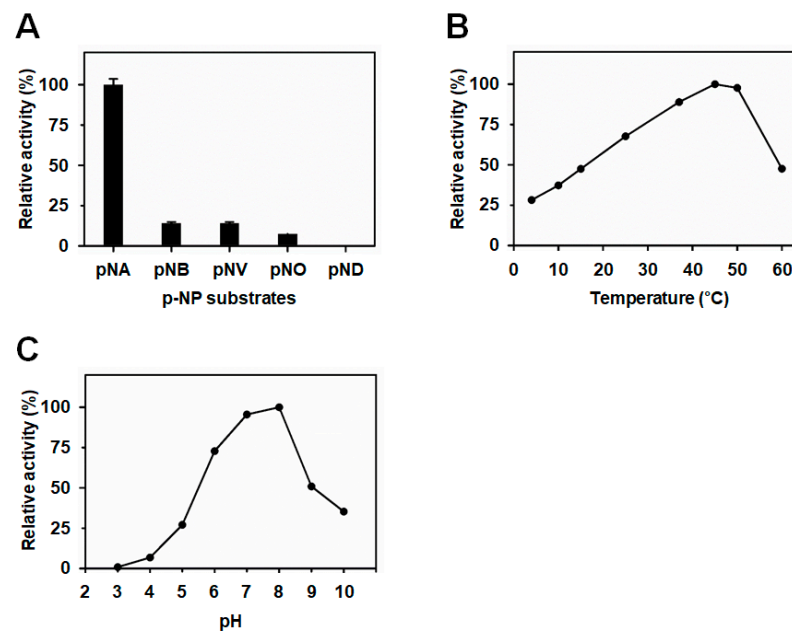


Figure 2. Biochemical characterization of *Burkholderiaceae* sp. S-formylglutathione hydrolase (*BuSFGH*). (A) Substrate specificity was investigated using p-nitrophenyl esters with different acyl-chain lengths. (B) Enzyme activity change of *BuSFGH* was monitored at different temperatures (4–60 °C). (C) Enzyme activity change of *BuSFGH* was monitored at different pHs (pH 3.0–pH 10.0).

Table 2. Structural homolog search results for *BuSFGH*, from a DALI search (DALI-Lite server).

Protein	PDB Code	DALI Z-Score	UniProtKB Code	Sequence % ID with <i>BuSFGH</i> (Aligned Residue Number)	Oligomerization State	Reference
Esterase from the oil-degrading bacterium <i>Oleispira antarctica</i>	3I6Y	47.7	D0VWZ4	53 (276/278)	Dimer	[28]
human esterase D	3FCX	47.4	P10768	56 (274/275)	Dimer	[29]
S-formylglutathione hydrolase homolog from <i>Shewanella frigidimarina</i>	6JZL	46.8	Q07XK4	55 (275/278)	Dimer	[9]
S-formylglutathione hydrolase from <i>Pseudoalteromonas haloplanktis</i>	3LS2	46.7	Q3IL66	49 (274/278)	Dimer	[6]
S-Formylglutathione Hydrolase from <i>Agrobacterium tumefaciens</i>	3E4D	45.7	A9CJ11	46 (277/278)	Dimer	[30]
Esterase D from <i>Neisseria meningitidis</i>	4B6G	45.7	Q9JZ43	52 (274/275)	Monomer	[1]
S-formylglutathione hydrolase from <i>Saccharomyces cerevisiae</i>	3C6B	42.5	P40363	42 (276/291)	Dimer	[31]

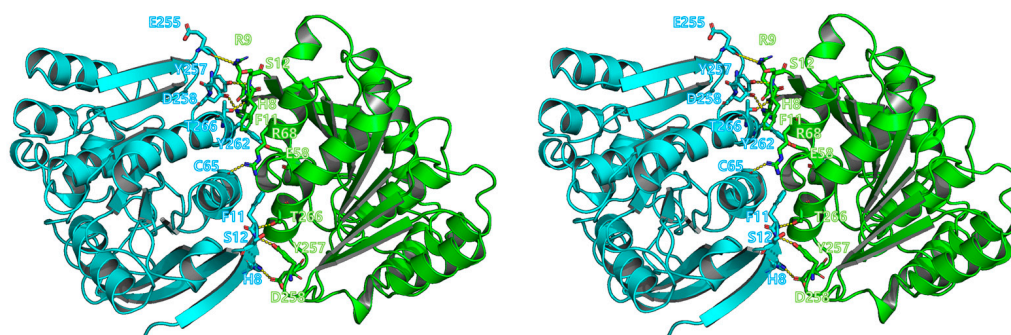


Figure 4. Dimerization of *Burkholderiaceae* sp. S-formylglutathione hydrolase (*BuSFGH*). The dimer interface in *BuSFGH* is shown in stereo view and interface residues are marked using a stick model. Interactions are shown as yellow-dotted lines.

3.4. Computational Modeling of *p*-NA-Bound *BuSFGH*

From the results of the enzyme activity assay, it was found that *BuSFGH* prefers the *p*-NA substrate, and based on this fact, a *p*-NA-bound *BuSFGH* structure model was produced using computational docking simulation. In the *p*-NA-bound *BuSFGH* model structure, the nitro group of the 4-nitrophenol ring moves towards the outside solvent region, and the opposite position of the hydroxyl group on the benzene ring directs the active site of *BuSFGH*. The benzene ring of *p*-NA interacts with the hydrophobic pocket region of *BuSFGH* via several hydrophobic residues (Trp96, Trp182, and Phe228). As a result, the carboxyl group in *p*-NA forms a close interaction with the catalytic Ser148 residue (3.27 Å distance) (Figure 5A,B). Previous structural and biochemical studies on yeast *ySFGH* from *S. cerevisiae* indicated that the backbone amide NH groups of Leu58 and Met162 form the oxyanion hole and stabilize the transition state of the substrate [31]. Consistent with this, the oxygen atom in the carbonyl group of *p*-NA interacted with the backbone nitrogen atom of Leu53 and was positioned close to the backbone of Met149 (corresponding to Leu58 or Met162 in *ySFGH*, respectively). Thus, it is suspected that the catalytic Ser148 residue forms an acyl-enzyme intermediate during *p*-NA cleavage, and the backbone nitrogen of Leu53 and Met149 residues may function as an oxyanion hole by stabilizing the negatively charged region of the transition state during *p*-NA hydrolysis (Figure 5C).

In this study, we characterized the *BuSFGH* enzyme using crystal structure determination and biochemical activity assays. The results showed that *BuSFGH* has high enzymatic specificity for short-length substrates. To obtain better structural insights into the substrate-binding mode and substrate preference of *BuSFGH*, we performed a computational molecular docking analysis using the *BuSFGH* apo-structure and *p*-NA. In conclusion, the substrate-binding site of *BuSFGH* was not large enough to accommodate substrates (*p*-NB, *p*-NV, *p*-NO, and *p*-ND) longer than *p*-NA. We also found that several hydrophobic residues (Trp96, Trp182, and Phe228) played important roles in the substrate binding of *BuSFGH*. Notably, *BuSFGH* contains a Trp96 residue in the substrate-binding region, whereas other bacterial SFGHs (*VaSFGH* and *SfSFGH*) have a Tyr residue at the corresponding position. The enzyme activity assay results for *BuSFGH* showed slightly different substrate preferences than those of *VaSFGH* and *SfSFGH*. *BuSFGH* enzymatic activity rapidly decreased as the substrate length increased, while *VaSFGH* and *SfSFGH* enzymatic activity gradually decreased as the substrate length increased. Therefore, it is possible that the Trp96 residue in *BuSFGH* contributes more to enzyme activity and substrate-binding differences than the Tyr residue in the other bacterial SFGHs.

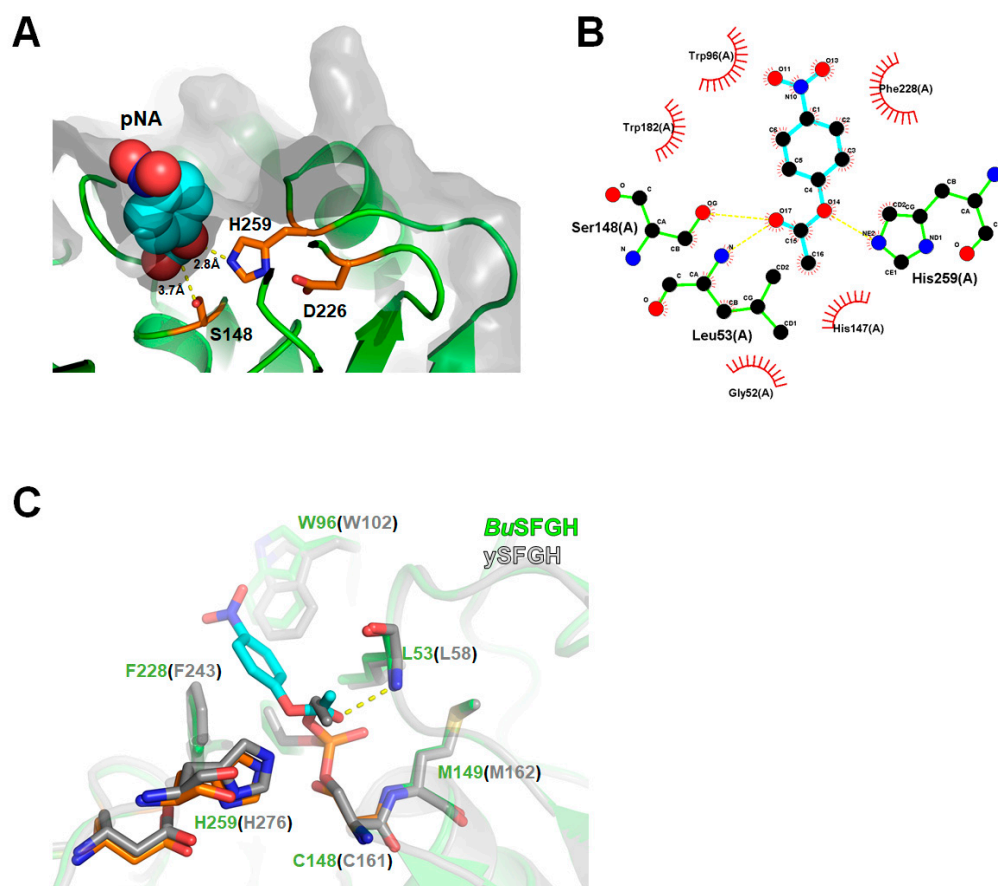


Figure 5. Computational docking model structure of p-NA-bound *Burkholderiaceae* sp. S-formylglutathione hydrolase (*BuSFGH*). (A) The p-NA (space-filling model) binding mode in *BuSFGH*. (B) The bound p-NA molecule and interacting residues of *BuSFGH* are shown as a LigPlot diagram. Hydrogen bonds are represented as green-dashed lines, and hydrophobic interactions are shown as red arcs. (C) Superimposed side chain representation of active site residues of *BuSFGH* (green) and *ySFGH* (gray). 2-Amino-3-(Diethoxy-Phosphoryloxy)-Propionic Acid (reaction product of paraoxon) complexed with *ySFGH* (PDB code: 3C6B) was used for superimposition and is represented with ribbon and stick model. Hydrogen bonding is indicated with yellow-dotted lines.

Author Contributions: Conceptualization, Y.-S.S. and J.H.L.; Methodology, J.H. and H.D.; Validation, Y.-S.S. and J.H.L.; Resources, Y.-S.S. and J.H.L.; Writing—Original Draft Preparation, J.H., H.D. and Y.-S.S.; Writing—Review and Editing, Y.-S.S. and J.H.L.; Funding Acquisition, Y.-S.S. All authors have read and agreed to the published version of the manuscript.

Funding: This work was supported by the Sun Moon University Research Grant of 2019.

Data Availability Statement: Not applicable.

Acknowledgments: We would like to thank the staff at the X-ray core facility of the Korea Basic Science Institute (KBSI; Ochang, Korea) and BL-5C of the Pohang Accelerator Laboratory (Pohang, Korea) for their kind help with the data collection.

Conflicts of Interest: The authors declare no conflict of interest.

References

- Chen, N.H.; Couñago, R.M.; Djoko, K.Y.; Jennings, M.P.; Apicella, M.A.; Kobe, B.; McEwan, A.G. A glutathione-dependent detoxification system is required for formaldehyde resistance and optimal survival of *Neisseria meningitidis* in biofilms. *Antioxid. Redox Signal.* **2013**, *18*, 743–755. [[CrossRef](#)] [[PubMed](#)]
- Chen, N.H.; Djoko, K.Y.; Veyrier, F.J.; McEwan, A.G. Formaldehyde stress responses in bacterial pathogens. *Front. Microbiol.* **2016**, *7*, 257. [[CrossRef](#)] [[PubMed](#)]

3. Cummins, I.; McAuley, K.; Fordham-Skelton, A.; Schwoerer, R.; Steel, P.G.; Davis, B.G.; Edwards, R. Unique regulation of the active site of the serine esterase S-formylglutathione hydrolase. *J. Mol. Biol.* **2006**, *359*, 422–432. [[CrossRef](#)] [[PubMed](#)]
4. Harms, N.; Ras, J.; Reijnders, W.N.; van Spanning, R.J.; Stouthamer, A.H. S-formylglutathione hydrolase of *Paracoccus denitrificans* is homologous to human esterase D: A universal pathway for formaldehyde detoxification? *J. Bacteriol.* **1996**, *178*, 6296–6299. [[CrossRef](#)] [[PubMed](#)]
5. Akoh, C.C.; Lee, G.C.; Liaw, Y.C.; Huang, T.H.; Shaw, J.F. GDSL family of serine esterases/lipases. *Prog. Lipid Res.* **2004**, *43*, 534–552. [[CrossRef](#)]
6. Alterio, V.; Aurilia, V.; Romanelli, A.; Parracino, A.; Saviano, M.; D’Auria, S.; De Simone, G. Crystal structure of an S-formylglutathione hydrolase from *Pseudoalteromonas haloplanktis* TAC125. *Biopolymers* **2010**, *93*, 669–677. [[CrossRef](#)]
7. Kordic, S.; Cummins, I.; Edwards, R. Cloning and characterization of an S-formylglutathione hydrolase from *Arabidopsis thaliana*. *Arch. Biochem. Biophys.* **2002**, *399*, 232–238. [[CrossRef](#)]
8. Legler, P.M.; Leary, D.H.; Hervey, W.J., 4th; Millard, C.B. A role for His-160 in peroxide inhibition of *S. cerevisiae* S-formylglutathione hydrolase: Evidence for an oxidation sensitive motif. *Arch. Biochem. Biophys.* **2012**, *528*, 7–20. [[CrossRef](#)]
9. Lee, C.W.; Yoo, W.; Park, S.H.; Le, L.T.H.L.; Jeong, C.S.; Ryu, B.H.; Shin, S.C.; Kim, H.W.; Park, H.; Kim, K.K.; et al. Structural and functional characterization of a novel cold-active S-formylglutathione hydrolase (SfSFGH) homolog from *Shewanella frigidimarina*, a psychrophilic bacterium. *Microb. Cell Fact.* **2019**, *18*, 140. [[CrossRef](#)]
10. Fellner, M.; Lentz, C.S.; Jamieson, S.A.; Brewster, J.L.; Chen, L.; Bogyo, M.; Mace, P.D. Structural basis for the inhibitor and substrate specificity of the unique Fph serine hydrolases of *Staphylococcus aureus*. *ACS Infect. Dis.* **2020**, *6*, 2771–2782. [[CrossRef](#)]
11. Miller, J.J.; Shah, I.T.; Hatten, J.; Barekattain, Y.; Mueller, E.A.; Moustafa, A.M.; Edwards, R.L.; Dowd, C.S.; Hoops, G.C.; Johnson, R.J.; et al. Structure-guided microbial targeting of antistaphylococcal prodrugs. *eLife* **2021**, *10*, e66657. [[CrossRef](#)]
12. Hwang, J.; Kim, B.; Lee, M.J.; Nam, Y.; Youn, U.J.; Lee, C.S.; Oh, T.J.; Park, H.H.; Do, H.; Lee, J.H. Structural basis for the substrate specificity of an S-formylglutathione hydrolase derived from *Variovorax* sp. PAMC 28711. *Biochem. Biophys. Res. Commun.* **2022**, *629*, 159–164. [[CrossRef](#)]
13. Otwinowski, Z.; Minor, W. Processing of X-ray diffraction data collected in oscillation mode. *Methods Enzymol.* **1997**, *276*, 307–326. [[CrossRef](#)]
14. Matthews, B.W. Solvent content of protein crystals. *J. Mol. Biol.* **1968**, *33*, 491–497. [[CrossRef](#)]
15. Read, R.J. Pushing the boundaries of molecular replacement with maximum likelihood. *Acta Crystallogr. D Biol. Crystallogr.* **2001**, *57*, 1373–1382. [[CrossRef](#)]
16. Winn, M.D.; Ballard, C.C.; Cowtan, K.D.; Dodson, E.J.; Emsley, P.; Evans, P.R.; Keegan, R.M.; Krissinel, E.B.; Leslie, A.G.; McCoy, A.; et al. Overview of the CCP4 suite and current developments. *Acta Crystallogr. D Biol. Crystallogr.* **2011**, *67*, 235–242. [[CrossRef](#)]
17. Emsley, P.; Cowtan, K. Coot: Model-building tools for molecular graphics. *Acta Crystallogr. D Biol. Crystallogr.* **2004**, *60*, 2126–2132. [[CrossRef](#)]
18. Murshudov, G.N.; Skubák, P.; Lebedev, A.A.; Pannu, N.S.; Steiner, R.A.; Nicholls, R.A.; Winn, M.D.; Long, F.; Vagin, A.A. REFMAC5 for the refinement of macromolecular crystal structures. *Acta Crystallogr. D Biol. Crystallogr.* **2011**, *67*, 355–367. [[CrossRef](#)]
19. Afonine, P.V.; Grosse-Kunstleve, R.W.; Echols, N.; Headd, J.J.; Moriarty, N.W.; Mustyakimov, M.; Terwilliger, T.C.; Urzhumtsev, A.; Zwart, P.H.; Adams, P.D. Towards automated crystallographic structure refinement with phenix.refine. *Acta Crystallogr. D Biol. Crystallogr.* **2012**, *68*, 352–367. [[CrossRef](#)]
20. Chen, V.B.; Arendall, W.B., 3rd; Headd, J.J.; Keedy, D.A.; Immormino, R.M.; Kapral, G.J.; Murray, L.W.; Richardson, J.S.; Richardson, D.C. MolProbity: All-atom structure validation for macromolecular crystallography. *Acta Crystallogr. D Biol. Crystallogr.* **2010**, *66*, 12–21. [[CrossRef](#)]
21. DeLano, W.L. *The PyMOL Molecular Graphics System*; DeLano Scientific LLC: San Carlos, CA, USA, 2002.
22. Schuck, P. Size-distribution analysis of macromolecules by sedimentation velocity ultracentrifugation and Lamm equation modeling. *Biophys. J.* **2000**, *78*, 1606–1619. [[CrossRef](#)] [[PubMed](#)]
23. Krissinel, E.; Henrick, K. Inference of macromolecular assemblies from crystalline state. *J. Mol. Biol.* **2007**, *372*, 774–797. [[CrossRef](#)] [[PubMed](#)]
24. Morris, G.M.; Huey, R.; Lindstrom, W.; Sanner, M.F.; Belew, R.K.; Goodsell, D.S.; Olson, A.J. AutoDock4 and AutoDockTools4: Automated docking with selective receptor flexibility. *J. Comput. Chem.* **2009**, *30*, 2785–2791. [[CrossRef](#)] [[PubMed](#)]
25. Lebedev, A.A.; Young, P.; Isupov, M.N.; Moroz, O.V.; Vagin, A.A.; Murshudov, G.N. JLigand: A graphical tool for the CCP4 template-restraint library. *Acta Crystallogr. D Biol. Crystallogr.* **2012**, *68*, 431–440. [[CrossRef](#)] [[PubMed](#)]
26. Trott, O.; Olson, A.J. AutoDock Vina: Improving the speed and accuracy of docking with a new scoring function, efficient optimization, and multithreading. *J. Comput. Chem.* **2010**, *31*, 455–461. [[CrossRef](#)]
27. Holm, L.; Rosenström, P. Dali server: Conservation mapping in 3D. *Nucleic Acids Res.* **2010**, *38*, W545–W549. [[CrossRef](#)]
28. Lemak, S.; Tchigvintsev, A.; Petit, P.; Flick, R.; Singer, A.U.; Brown, G.; Evdokimova, E.; Egorova, O.; Gonzalez, C.F.; Chernikova, T.N.; et al. Structure and activity of the cold-active and anion-activated carboxyl esterase OLEI01171 from the oil-degrading marine bacterium *Oleispira antarctica*. *Biochem. J.* **2012**, *445*, 193–203. [[CrossRef](#)]
29. Wu, D.; Li, Y.; Song, G.; Zhang, D.; Shaw, N.; Liu, Z.J. Crystal structure of human esterase D: A potential genetic marker of retinoblastoma. *FASEB J.* **2009**, *23*, 1441–1446. [[CrossRef](#)]

30. van Straaten, K.E.; Gonzalez, C.F.; Valladares, R.B.; Xu, X.; Savchenko, A.V.; Sanders, D.A. The structure of a putative S-formylglutathione hydrolase from *Agrobacterium tumefaciens*. *Protein Sci.* **2009**, *18*, 2196–2202. [[CrossRef](#)]
31. Legler, P.M.; Kumaran, D.; Swaminathan, S.; Studier, F.W.; Millard, C.B. Structural characterization and reversal of the natural organophosphate resistance of a D-type esterase, *Saccharomyces cerevisiae* S-formylglutathione hydrolase. *Biochemistry* **2008**, *47*, 9592–9601. [[CrossRef](#)]

Disclaimer/Publisher’s Note: The statements, opinions and data contained in all publications are solely those of the individual author(s) and contributor(s) and not of MDPI and/or the editor(s). MDPI and/or the editor(s) disclaim responsibility for any injury to people or property resulting from any ideas, methods, instructions or products referred to in the content.